Arabian Journal of Chemistry (2017) **10**, 215–225

King Saud University

Arabian Journal of Chemistry

www.ksu.edu.sa
www.sciencedirect.com

ORIGINAL ARTICLE

Green synthesis: *In-vitro* anticancer activity of copper oxide nanoparticles against human cervical carcinoma cells

P.C. Nagajyothi [a,1], P. Muthuraman [b,1], T.V.M. Sreekanth [c], Doo Hwan Kim [b], Jaesool Shim [a,*]

[a] *School of Mechanical Engineering, Yeungnam University, 214-1 Dae-dong, Gyeongsan-si, Gyeongsangbuk-do 712-749, Republic of Korea*
[b] *Dept of Bioresources and Food Science, Konkuk University, Seoul, Republic of Korea*
[c] *School of Chemical Engineering, Yeungnam University, 214-1 Dae-dong, Gyeongsan-si, Gyeongsangbuk-do 712-749, Republic of Korea*

Received 3 November 2015; accepted 28 January 2016
Available online 4 February 2016

KEYWORDS

Copper oxide nanoparticles;
Black beans;
HeLa cells;
In-vitro anticancer

Abstract Copper oxide nanoparticles (CuO NPs) were synthesized by a green route using an aqueous black bean extract and characterized by XRD, FT-IR, XPS, Raman spectroscopy, DLS, TEM, SAED, SEM, and EDX. The synthesized CuO NPs were spherical in shape, and the XRD results show the average size of the NPs was ~26.6 nm. The cytotoxic effect of the CuO NPs was determined by sulforhodamine-B assay. Mitochondria-derived reactive oxygen species (ROS) were increased and initiated lipid peroxidation of the liposomal membrane, which regulates several signaling pathways and influences the cytokinetic movements of cells. Mitochondrial fragmentation disruption assay confirmed the alteration in the mitochondrial structure after incubation with nanoparticles. In addition, clonogenic assay confirmed the inability of NPs incubated cancer cells to proliferate well. Our experimental results show that the CuO NPs can induce apoptosis and suppress the proliferation of HeLa cells.

* Corresponding author. Tel.: +82 53 810 2465; fax: +82 53 810 4627.
E-mail addresses: tvmsreekanth@gmail.com (T.V.M. Sreekanth), jshim@ynu.ac.kr (J. Shim).
[1] These authors contributed equally to this work.
Peer review under responsibility of King Saud University.

Production and hosting by Elsevier

1. Introduction

Cancer is one of the leading causes of death worldwide and is characterized by proliferation of abnormal cells. Surgery, chemotherapy, and radiotherapy methods are used in cancer treatment. However, these standard methods are expensive and have side effects with limitations of their use, so there is an urgent need for effective, inexpensive and non-toxic, treatments with minimal side effects that are acceptable by people. Nanoscale material structures usually range from 1 to 100 nanometers (nm) in size, comparable to large biological molecules

http://dx.doi.org/10.1016/j.arabjc.2016.01.011
1878-5352

(enzymes, receptors, etc.). Nanoparticles (NPs) can offer unique interactions with biomolecules and may be useful in cancer diagnosis and treatment (Seigneuric et al., 2010; Liu et al., 2010).

CuO is an important p-type semiconductor with a band gap of ~1.7 eV (Tadjarodi and Roshani, 2014). It is extensively used for a wide range applications, such as high-temperature superconductors (Yu and Zhang, 2009), solar cells (Rahnama and Gharagozlou, 2012), gas sensors (Zhu et al., 2007), catalytic applications (Chen et al., 2011; Nasrollahzadeh et al., 2015a,b,c,d,e,f,g), optical applications (Yu et al., 2004), hydrogen storage materials (Safarifard and Morsali, 2012) and medical applications. Several methods have been used for the synthesis of CuO NPs, including sol–gel (Eliseev et al., 2010), electrochemical (Borgohain et al., 2000), thermal decomposition (Salavati and Davar, 2009), microwave irradiation (Wang et al., 2002), solid state reactions (Xu et al., 2000), precipitation (Siddique and Karmakar, 2013), solution combustion methods (Umadevi and Christy, 2013), ultrasonic mixing and self-assembly methods (Shende et al., 2008), and hydrothermal route in the presence of PEG (Cao et al., 2004). These methods involve high temperature, high pressure and hazardous chemicals, and some toxic chemicals absorbed on the surface of NPs may cause adverse medical effects (Nasrollahzadeh, 2014). Therefore, it is a challenge to find a convenient, rapid, mild, non-toxic and natural product to produce metal/metal–oxide NPs in an aqueous environment (Iravani, 2011; Huang et al., 2011; Nasrollahzadeh and Sajadi, 2015; Zhan et al., 2011; Nasrollahzadeh et al., 2015a,b,c,d,e,f,g). Bacteria, fungi, algae, and plants are used for NP preparation, but a synthesis of NPs from plants is more stable, allows different sizes and shapes, is inexpensive, and is faster than in the case of microorganisms (Table 1). Green synthesis of nanoparticles has several advantages over chemical and physical synthesis, such as simplicity and eco-friendly (Nasrollahzadeh et al., 2015a,b,c,d,e,f,g; Abdel-Halim et al., 2011; Wang et al., 2014; Dubey et al., 2010).

Black beans (*Phaseolus vulgaris* family: Fabaceae) have high amounts of anthocyanin, protein, vitamins A, B, and C, calcium, and polyphenols. Polyphenolic compounds are used to reduce diseases caused by reactive oxygen and nitrogen species (Maestri et al., 2006). These compounds decrease the risk of cardiovascular diseases, obesity, cancers, and diabetes (Dzomba et al., 2013). In the present study, we report the green synthesis of CuO NPs using an aqueous black bean extract and evaluate its anticancer activity in human cervical cancer (HeLa) cells.

2. Materials and methods

2.1. Materials

Dry black beans were collected from a local supermarket in Gyeongsan-si, South Korea. Copper sulfate ($CuSO_4 \cdot 5H_2O$) was purchased from Sigma–Aldrich, Seoul, South Korea. Dimethyl sulphoxide (DMSO) and sulforhodamine B (SRB) were purchased from Sigma. Dulbecco's Modified Eagle's Medium (DMEM), fetal bovine serum (FBS), penicillin–streptomycin and trypsin-EDTA were obtained from Welgene (Daegu, South Korea). Mito Tracker Red, Hoechst 33252 and 2′, 7′-Dichlorofluorescin diacetate (DCFH-DA) were purchased from Santa Cruz Biotechnology, Inc. (Santa Cruz, California, USA).

2.2. Synthesis of CuO NPs

Ten grams of beans were washed with distilled water to remove any dust and adhesive materials and made into a paste by mortar and pestle. This paste was moved to a 250-ml beaker, which was filled with distilled water to a final volume of 100 ml. This was heated up to 80 °C for around 30–40 min, allowed cool to room temperature, filtered using Whatman filter paper, and stored in a refrigerator for further study.

To synthesize CuO NPs, we used a literature method (Sivaraj et al., 2014a,b) with slight modifications. To the 100 ml of bean extract, we added required quantities of $CuSO_4$ to attain 10 mM. The reaction mixture was stirred for around 20 min to mix completely the metal precursor and kept in an oil bath with vigorous stirring at 120 °C for 7–8 h. The reaction mixture was cooled to room temperature, and a brown–black colored product was obtained. The solid product was separated by centrifuge (15,000 rpm, 15 min, 4 °C), washed with DI water twice, and calcined at 400 °C for 2 h. The final CuO NPs powder was stored in a vacuum desiccator for further use.

2.3. Characterization of CuO NPs

The purity and grain size of the green-synthesized CuO NPs were characterized by X-ray diffraction (PANalytical X'Pert MRD) using Cu Kα radiation ($\lambda = 1.54$ Å) at 40 kV and 30 mA. Functional groups and chemical composition were analyzed by Fourier transform infrared spectroscopy (FT-IR, Perkin–Elmer-Spectrum Two). The spectrum was obtained by recording at a wavelength of 400–4000 cm^{-1}. Raman spectroscopy was performed using a Horiba, XploRA Series, PLUS. Dynamic light scattering (DLS) was performed with DynaPro Plate Reader (Wyatt Technology). The chemical state and composition of the elements present in the CuO NPs were examined by X-ray photoelectron spectroscopy (XPS, Thermo Scientific K-Alpha) using an Al Kα X-ray source (1486.6 eV). The source energies of 200 eV and 30 eV were used for the high and low-resolution scans, respectively. The shape and morphology of the CuO NPs were determined by scanning electron microscopy (SEM-Hitachi s-4200 N), and energy dispersive X-ray analysis (EDAX) and elemental mapping were done using the same instrument. High-resolution transmission electron microscopy (HR-TEM–FEI-Tecnai TF 20) and selected area diffraction (SAED) were also performed.

2.4. Cell culture

HeLa cells were obtained from the Korean Cell Line Bank (South Korea). Cells were maintained in growth medium supplemented with 10% FBS and 1% antibiotics (penicillin–streptomycin). The cells were grown in a CO_2 incubator at 37 °C with 5% CO_2.

2.5. SRB assay

HeLa cells were seeded at a density of 2.5×10^4 cells/well into 96-well plates and allowed to adhere for 24 h at 37 °C. Cells were treated with CuO NPs at different concentrations (0.001, 0.01, 0.1, 0.5 and 1 mg/ml) for 12, 24 and 48 h. At the end of the treatment duration, the cytotoxic effect on the HeLa cells was measured by SRB assay (Pandurangan et al., 2015a,b).

2.6. Determination of ROS production

HeLa cells were seeded in 96-well plates in growth medium at a cell density of 5000 cells per well and incubated at 37 °C and 5% CO_2. After 24 h of adherence, cells were treated with

Table 1 CuO NPs synthesized by green route.

Plant name	Shape	Size (nm)	Significance	References
Malva sylvestris leaf	Spherical	5–30	Antibacterial activity Shigella and listeria bacteria	Awwad et al. (2015)
Calotropis gigantean leaf	Spherical	20	Solar cells applications	Sharma et al. (2015)
Aloe vera leaf	Spherical	20–30	Antibacterial activity against fish bacterial pathogens	Vijay Kumar et al. (2015)
Rubus glaucus leaf and fruit	Spherical	43.3	Antioxidant was evaluated against DPPH	Brajesh Kumar et al. (2015)
Albizia lebbeck leaf	Spherical	< 100	–	Jayakumarai et al. (2015)
Rosa Sahandina fruit	Spherical	< 50	–	Saeed et al. (2014)
Tabernaemontana divaricate leaf	Spherical	48	Antibacterial activity against urinary tract pathogen	Sivaraj et al. (2014a, b)
Acalypha indica leaf	Spherical	29	Antibacterial and antifungal effect against *Escherichia coli*, *Pseudomonas fluorescens* and *Candida albicans*. Anti-cancer activity against MCF-7 human breast cancer cell line	Sivaraj et al. (2014a, b)
Aloe barbadensis Miller	Versatile and spherical	15–30	–	Sangeetha et al. (2012)
Pterocarpus marsupium wood	Spherical	20–50	Antibacterial activities against *E. coli*, *P. vulgaris*, *K. pneumonia*, *S. aureus*, *S. epidermidis*, *B. cereus*	Rajgovind et al. (2015)
Pyrus pyrifolia leaves	Spherical	24	Photocatalytic study	Sundaramurthy and Parthiban (2015)

CuO NPs (0.5 and 1 mg/ml). At the end of treatment, cells were examined under a fluorescence microscope (Axiovert 2000, Carl Zeiss, Germany) (Pandurangan et al., 2015a,b).

2.7. Mitochondrial membrane disruption

To study the apoptosis-induction potential of CuO NPs by disrupting the mitochondrial membrane, we observed the changes in mitochondrial morphology following CuO NP treatment. HeLa cells were cultured at a density of 2.5×10^4 cells/well and grown in the culture medium. Cells were treated with CuO NPs for 24 h. At the end of 24 h, cells were washed with PBS and exposed to 50 nM Mito Tracker Red for 40 min at 37 °C and then washed and exposed to 1 μg/ml of Hoechst 33258 for 10 min at room temperature. Cells were washed with PBS and viewed under a fluorescent microscope (Axiovert 2000, Carl Zeiss, Germany). Hoechst 33258 staining visualizes the cell nuclei, and Mito Tracker Red stains the mitochondria to allow for visualizing alterations in mitochondrial structure due to the CuO NP treatment (Iovine et al., 2014).

2.8. Clonogenic assay

HeLa cells were cultured at a density of 2.5×10^4 cells/well in 6-well plates and allowed to adhere for 24 h. After adherence, cells were treated with CuO NPs for 24 h. The cells were washed with PBS and stained for 30 min with a solution of crystal violet (0.2%), methanol (50%), and acetic acid (10%) in water at room temperature. The cells were completely washed with deionized water and viewed under a light microscope (CKX41, Olympus, Japan) (Moktan and Raucher, 2012).

3. Results and discussion

3.1. Characterization of CuO NPs

The black bean contains a number of phytochemicals such as proteins, amino acids, oligosaccharides, complex carbohydrates, alkaloids, phenols, saponins, flavonoids, and among others (Geil and Anderson, 1994; Mishra et al., 2010). From the experimental findings, here we proposed one possible mechanism and possible stepwise pathway for the formation of CuO NPs (Scheme 1). At first, the metal precursor ($CuSO_4 \cdot 5H_2O$) reacts with hydroxyl anion (–OH) which is generated by water, and forms copper hydroxide (Cu $(OH)_2$). The aqueous extract of black bean contains a lot of phytochemicals such as proteins, amino acids, oligosaccharides, complex carbohydrates, alkaloids, phenols, saponins, and flavonoids, and these compounds will act as encapsulating agents and be reduced from copper hydroxide to copper oxide nanoparticles. The FT-IR bands located at 1037.6, 595.8, and 539.9 cm^{-1} have been assigned to N–H stretching vibrations of aliphatic amines (Salah-Eddin et al., 2015), C–Cl stretching of alkyl halides (GnanaDhas et al., 2012) and C–Br stretching of alkyl halides (Sankar Narayan et al., 2015) (Fig. 1a). The strong band located at 1037.6 cm^{-1}, whereas peaks at 595.8 and 539.9 cm^{-1} can be attributed to vibrations of CuO, confirming the formation of highly pure CuO NPs (Ren et al., 2009).

Raman spectroscopy is a very useful technique for the study of phases and structure of metal oxide systems. The Raman shift and bandwidth change with decreasing particle size (Swarnkar et al., 2009, 2011; Tanaka et al., 1992, 1993). Xu et al. (1999) reported that Raman intensity is related to the grain size. When grain sizes increases, Raman peaks become stronger and sharper and shift slightly to a higher wave

$$CuSO_4.\,5H_2O + 2OH^- \longrightarrow Cu(OH)_2 + SO_4^{2-} + 5H_2O$$

$$Cu(OH)_2 + \left[\begin{array}{c}\text{Amino acids}\\ + \\ \text{Alkyl halides}\end{array}\right] \longrightarrow CuO\ NPs + H_2O$$

Scheme 1 Possible mechanism for the formation of CuO NPs, from black bean aqueous extract.

number (Bhaumik et al., 2014). The Raman spectrum of the green-synthesized CuO NPs is shown in Fig. 1b. The spectrum contains three peaks located at 286, 336, and 623 cm^{-1}. The firm peak at 286 cm^{-1} and a weak peak at 336 cm^{-1} are assigned to CuO (Swarnkar et al., 2009). The peak at 286 cm^{-1} can be identified as the A_g mode, and the peaks at 336 and 623 cm^{-1} can be identified as B_g modes in the monoclinic CuO (Irwin et al., 1990). These wave numbers are close to those reported in the literature (Xu et al., 1999; Rashad et al., 2013).

Fig. 1c shows the XRD diffraction peaks at 2θ of 32.57, 34.33, 35.64, 38.80, 46.45, 48.87, 51.57, 53.52, 58.37, 61.72, 65.91, 66.29, 67.98, 68.17, 72.44, 75.06, and 75.30 °C, which were assigned to the (110), (002), (−111), (111), (−112), (−202), (112), (020), (202), (−113), (022) (−311), (220) (−221), (311) (004) and (−222) planes, respectively. The XRD spectrum revealed that CuO NPs have crystalline nature and monoclinic structure, which was confirmed by the International Center of Diffraction Data Card (JCPDS NO: 01-080-1268). No other phases were observed, indicating the purity of CuO NPs. The average crystalline size of CuO NPs was calculated using the Debye–Scherrer's equation (Cullity, 1978) as follows:

$$D = K\lambda/\beta\cos\theta \quad (1)$$

where K is Scherrer's constant ($K = 0.94$), D is the mean crystalline size, λ is the X-ray wavelength (0.1546 nm), β is the full-width at half-maximum of the XRD line in radians, and θ is the half diffraction angle. The average size of the greensynthesized CuO NPs was found be about ~26.6 nm. The XRD diffraction patterns shown in this study are in good agreement with the earlier research reported for the green synthesis of CuO NPs (Nasrollahzadeh et al., 2015a,b,c,d,e,f,g; Vijay Kumar et al., 2015). The DLS analysis was used to find out the average particle size of the green synthesized CuO NPs. Fig. 1d shows the average size distribution of CuO NPs ~35 nm.

The morphology of the CuO NPs was analyzed using SEM and HR-TEM. Fig. 2a shows the SEM images of the CuO NPs, and the particles are mostly spherical, hexagonal and

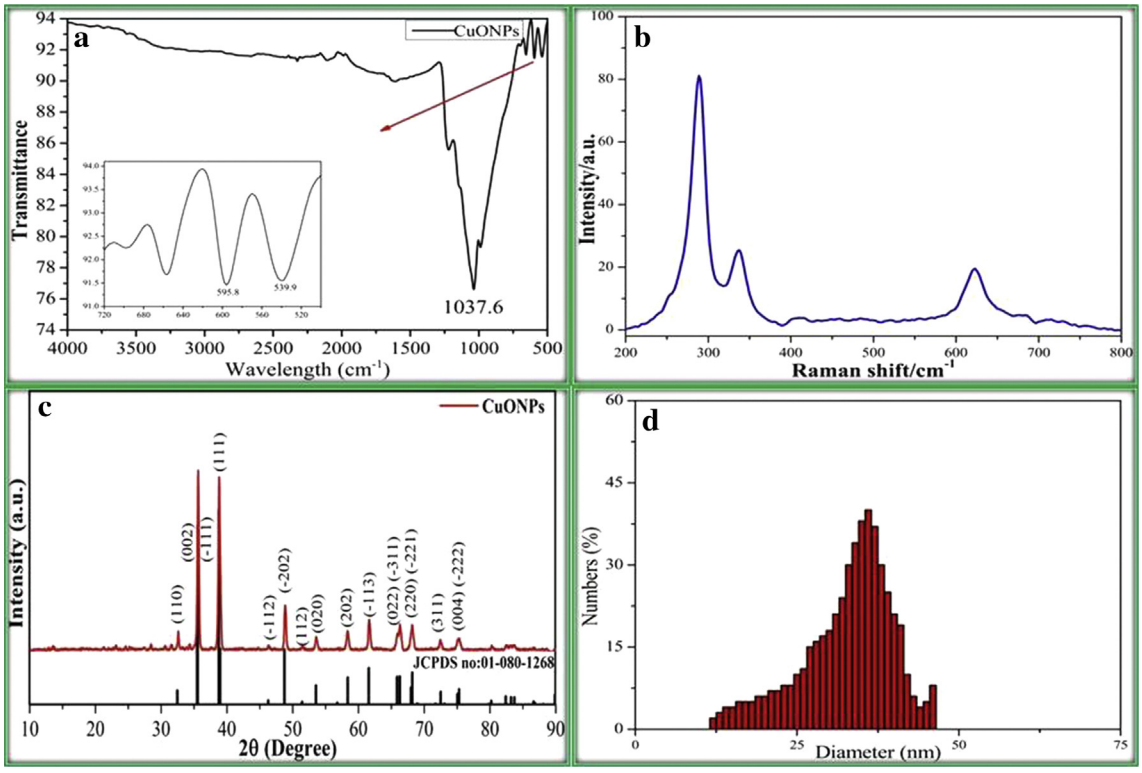

Figure 1 (a) FT-IR spectrum of green synthesized CuO NPs, (b) Raman spectrum of green synthesized CuO NPs, (c) XRD pattern of green synthesized CuO NPs and (d) DLS of green synthesized CuO NPs.

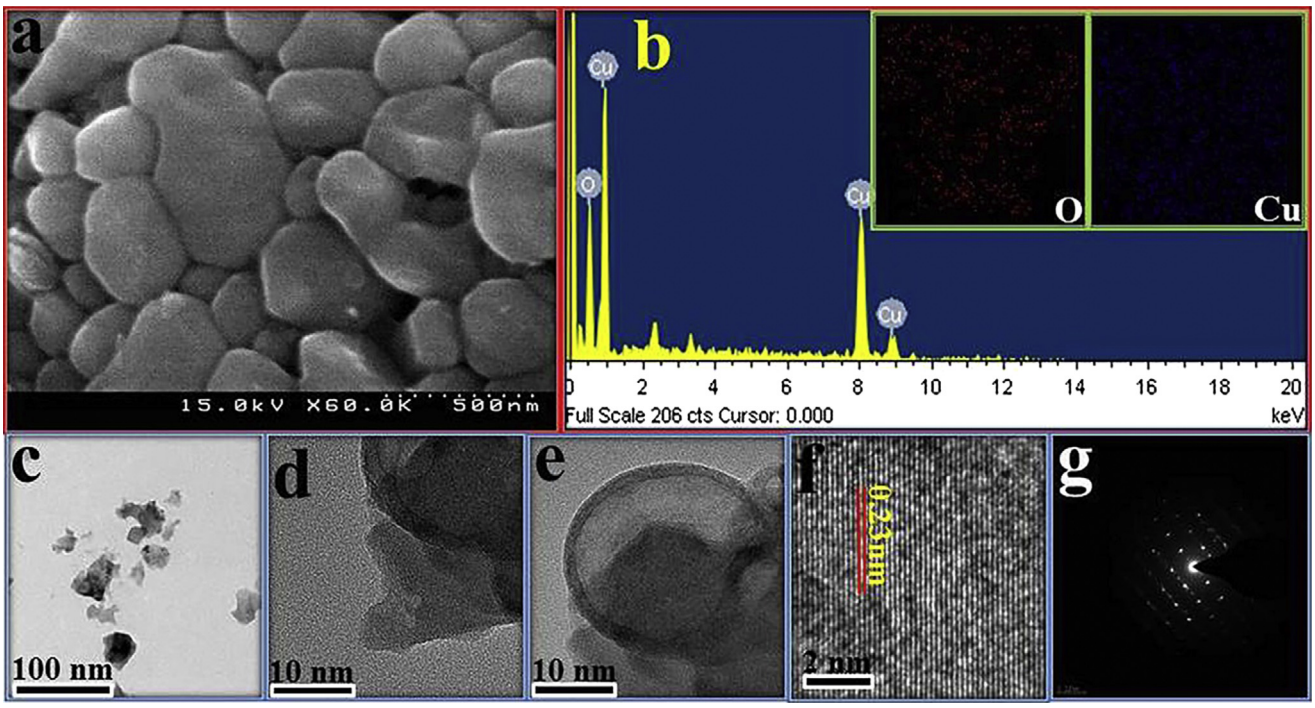

Figure 2 Microscopic images of green synthesized CuO NPs: (a) SEM image, (b) EDAX of green synthesized CuO NPs; inset: elemental mapping of oxygen and copper, (c–e) TEM images at different magnifications, (f) high magnification view of green synthesized CuO NPs and (g) SAED patter of green synthesized CuO NPs.

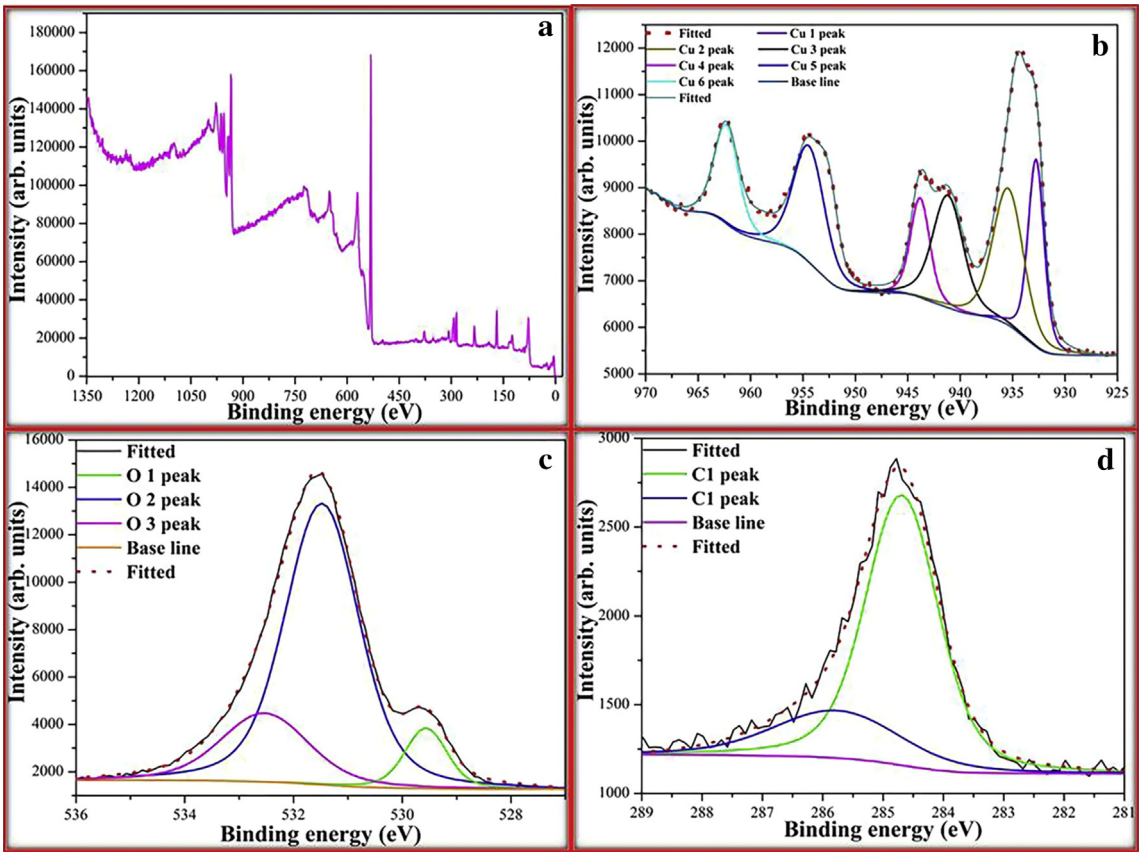

Figure 3 XPS analysis of green synthesized CuO NPs: (a) survey scan, and high-resolution scans of (b) Cu 2p, (c) O 1s and (d) C 1s.

uneven shapes. The copper (Cu) and oxide (O) peaks and elements were confirmed using EDAX analysis (Fig. 2b) and elemental mapping (inset of Fig. 2b). Nasrollahzadeh et al. (2015a,b,c,d,e,f,g) also confirmed the copper oxide composition in green synthesized CuO NPs through EDX. TEM images show that the CuO NPs are spherical (Fig. 2c–e). This is very similar to those described in the previous reports (Nasrollahzadeh et al., 2015a,b,c,d,e,f,g). Fig. 2f shows that the CuO NPs have a lattice d spacing of 2.3 Å in the (1 1 1) plane, confirming high crystallinity of the green-synthesized CuO NPs. The SAED pattern of the CuO NPs clearly shows the crystalline nature of the NPs (Fig. 2g).

Fig. 3 shows the XPS analysis of the NPs, and Fig. 3a shows the survey scan. All the indexed peaks correspond to Cu, C, and O. In the survey, the spectrum shows Cu photoelectron peaks (Cu3s, Cu2p, Cu3p, and its Cu LMM Auger), O peaks (O1s and its OKLL Auger), and the photoelectron peak of the adventitious carbon (C1s). No impurities on the surface of the NPs were detected, and the Cu and O elements result from the copper electrolytic plate and H_2O.

The high-resolution XPS spectra of the Cu 2p are shown in Fig. 3b with strong fitting peaks at around 932.7 and 935.5 eV for Cu $2p_{3/2}$ and 952.5 and 954.5 eV for Cu $2p_{1/2}$. These results are close to literature results (Gao et al., 2010). The gap between the Cu $2p_{3/2}$ and Cu $2p_{1/2}$ is 19.8 eV, which is in agreement with the standard value of 20.0 eV for CuO (Lin et al., 2004; Zhu et al., 2004). In addition to the Cu $2p_{3/2}$ and Cu $2p_{1/2}$ peaks, two shake-up satellite peaks appear at binding energies of 943.8 and 962.4 eV. The shake-up satellite peaks are evidence of an open $3d^9$ shell corresponding to the Cu^+ state.

Fig. 3c shows the high-resolution XPS spectra of O 1s. This core-level spectrum is broad and consists of three peaks that can be assigned to the O^{2-} in CuO NPs. The main peak at the lower binding energy of 529.4 eV is attributed to Cu–O, which is consistent with the literature (Liu et al., 2011). The other peaks at 531.4 and 532.5 eV could be assigned to chemisorbed oxygen caused by surface hydroxyl and correspond to O–H bonds (Liu et al., 2011) and –OH, respectively. Some water molecules were also physically adsorbed on the surface

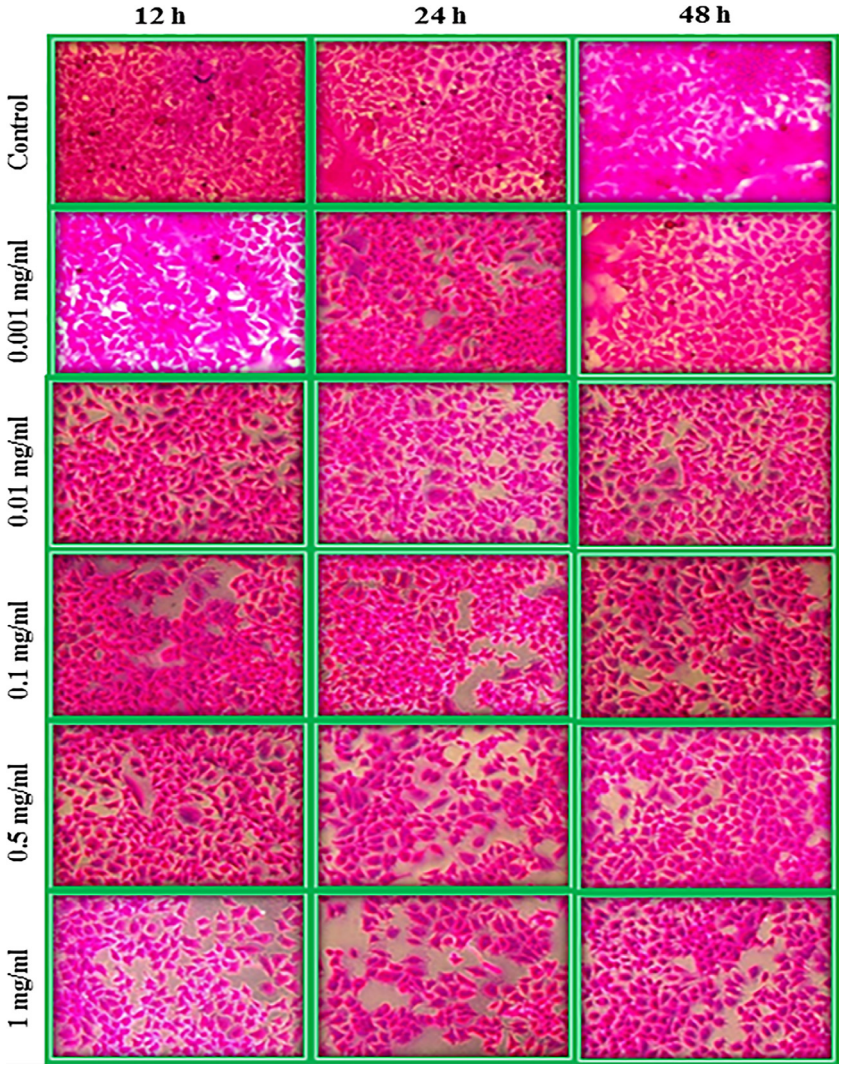

Figure 4 Cytotoxic effect of CuO NPs on HeLa cells by SRB assay at 12, 24 and 48 h. Results were expressed as a percentage of viability of HeLa cells compared to their control.

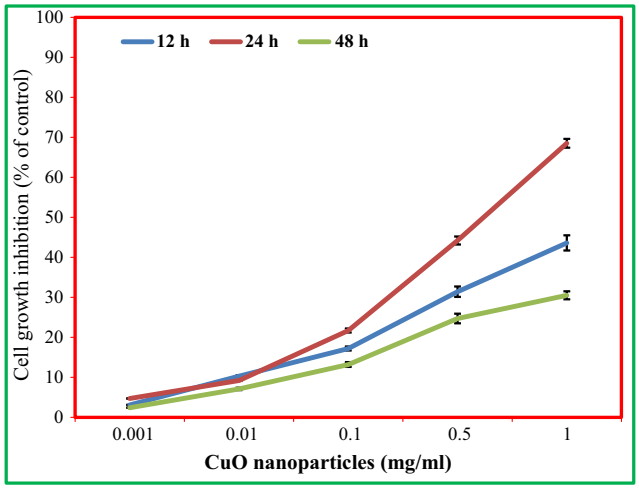

Figure 5 Cytotoxic effect of CuO NPs on HeLa cells by SRB assay at 12, 24 and 48 h. Results are expressed as a percentage of viability of HeLa cells compared to their control. The percentage of growth inhibition (c) was calculated as follows: growth inhibition (%): (control-sample/control) * 100. Values were expressed as means ± SEM.

of the NPs (Li et al., 2007). Fig. 3d shows the high-resolution XPS spectra of C 1s. This core-level spectrum is broad and consists of two peaks. The C element was due to the biomass material on the surface of NPs and the adsorbed carbon dioxide.

3.2. In-vitro anticancer studies

Black bean varieties contain a higher amount of bioactive compounds such as phenolic compounds (flavonoids, tannins, and anthocyanin), protease inhibitors, phytic acids, saponins and antioxidant properties compared to other common bean cultivars (Harland and Morris, 1995). Black bean extract containing 1–2% phytate, phytate and flavonoids inhibited the growth of breast, colon, liver and prostate cancer cells via apoptosis without interfering with the proliferation of normal human fibroblast (Bawadi, 2005; Bobe et al., 2008; Hangen and Bennik, 2002; Thompson et al., 2012). However, this black bean has been extensively studied for various anticancer studies; no work has been carried out on the CuO NPs synthesis and anticancer activity against HeLa cell line. Based on this reason we selected only black bean mediated CuO NPs in the anticancer studies.

CuO NPs showed a clear cytotoxic effect on HeLa cells and a clear concentration–response relationship (Figs. 4 and 5). 0.5 and 1 mg/ml of CuO NPs could inhibit the growth of HeLa cells. Therefore, 0.5 and 1 mg/ml of CuO NPs were used for further study. HeLa cells were treated with various concentrations of CuO NPs for 12, 24 and 48 h. Intracellular ROS generation was determined by the fluorescent probe DCFH-DA. Fluorescence study indicated that the green fluorescence

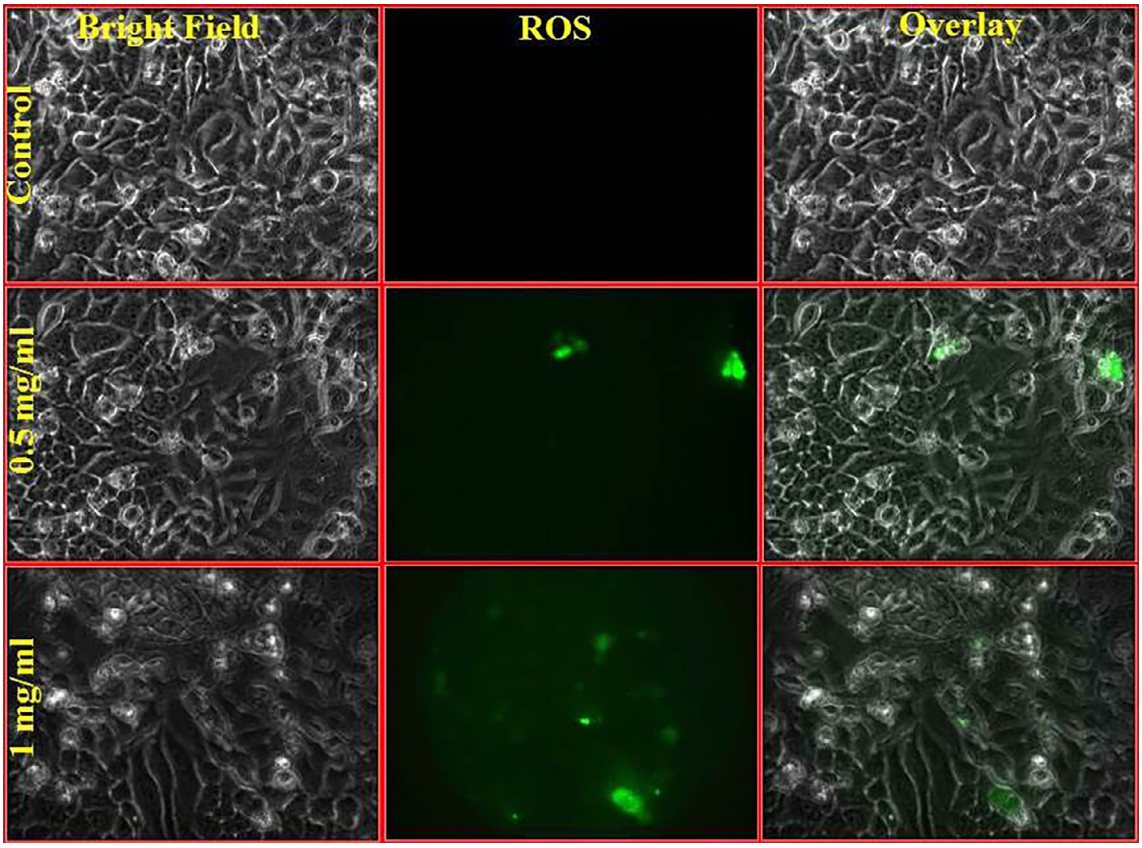

Figure 6 Effect of CuO NPs ROS level. HeLa cells were grown in 96 well plate and allowed to adhere for 24 h. Cells were treated with different concentration of CuO NPs for 24 h. At the end of 24 h, cells were treated with DCFH-DA and fluorescence of HeLa cells was measured at 495/525 nm in a fluorescent plate reader.

intensity of DCF was enhanced in the CuO NPs-treated cells compared with the control cells. These results indicated that CuO NPs induced intracellular ROS generation in a dose-dependent manner (Fig. 6).

The alteration in mitochondrial and nuclear morphology in response to the treatment was assessed by the Mito Tracker Red and Hoechst 33258, respectively. An extended lace-like network of normal mitochondria was found in control HeLa cells. CuO NP treatment significantly altered the mitochondrial morphology of normal HeLa cells. Mitochondria have condensed clump structures in carnosine-treated cancer cells (Fig. 7). Clonogenic survival assay was carried out to determine the ability of HeLa cells to proliferate and to form a large colony or a clone in the presence of 0.5 and 1 mg/ml CuO NPs. CuO NPs significantly reduced the number of colonies of cervical carcinoma cells compared to the control (Fig. 8).

Copper compounds have been used to treat cancer and several diseases for thousands of years (Hajra and Liu, 2004). Copper compounds may contain similar properties to arsenic trioxide, which is another anti-tumor compound (Wang and Chen, 2000). Copper is a well-known heavy metal that is toxic to mammalian cells. However, with the advancement of nanotechnology, the NPs can target specific cells with lesser side effects. Even though the copper compounds have strong therapeutic potential, no study has been reported at the *in vitro* level. Our results agree with the results of Mariappan et al.

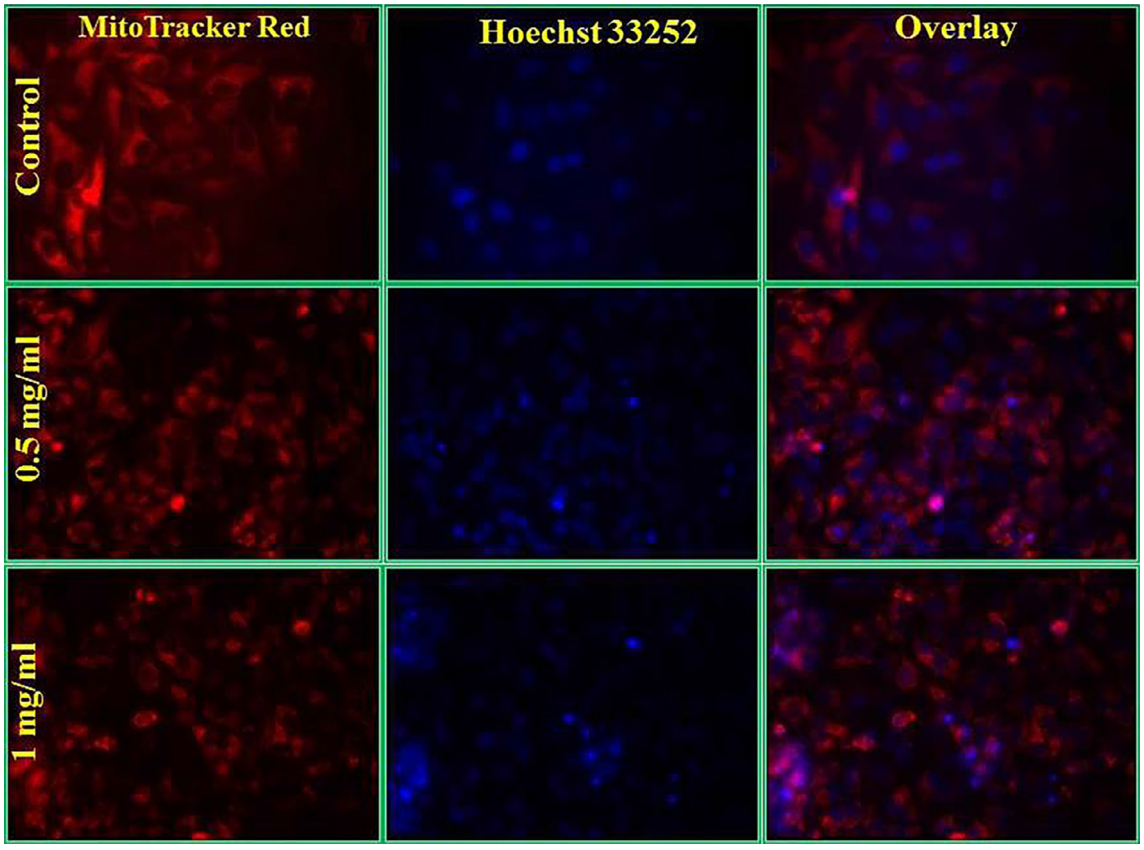

Figure 7 Effect of CuO NPs on mitochondria. Cells were stained with Mito Tracker® Red and Hoechst 33258 to image the mitochondria and nuclei, respectively. Condensed nuclei and clumped structure of mitochondria of HeLa cells indicate apoptotic cells were found.

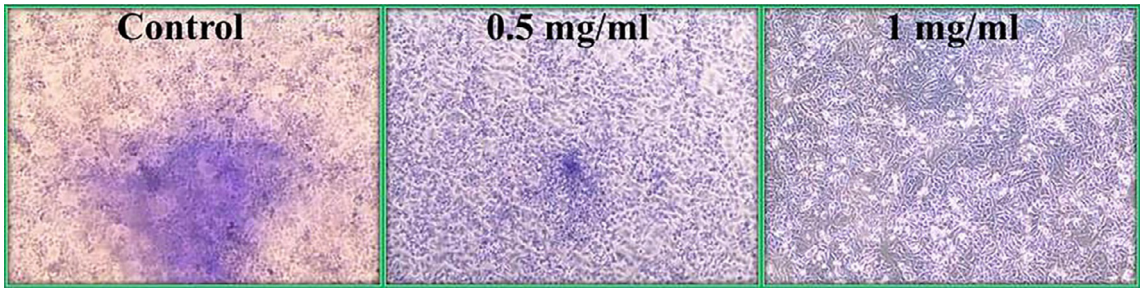

Figure 8 Effect of CuO NPs on clonogenic cell proliferation. Clonogenic survival assay on HeLa cells following incubation with CuO nanoparticles (0.5 & 1 mg/ml).

(2011), who reported that ZnO NPs kill human myeloblastic leukemia cells and are less toxic to normal peripheral blood mononuclear cells. Wu et al. (2011) reported that iron-core gold shell NPs have cell-specific cytotoxicity.

The NPs can suppress cell viability by different mechanisms such as apoptosis and necrosis (AshaRani et al., 2009). Apoptosis is a cell suicide mechanism that controls cell numbers. The apoptotic cascade can be triggered through extrinsic and intrinsic pathways (Kumar et al., 2011). The induction of tumor cell apoptosis is a crucial mechanism for an anticancer compound (Frankfurt and Krishan, 2003). Apoptosis process characterized by the morphological and biochemical changes and apoptosis of different cells in the same tissue does not occur at the same time. CuO NPs showed a clear cytotoxic effect on HeLa cells in SRB assay. In our study, copper oxide nanoparticles exerted a cytotoxic effect on HeLa cells in a concentration-dependent manner.

4. Conclusion

In-vitro anticancer results indicated that CuO NPs induced intracellular ROS generation in a dose-dependent manner and significantly reduced cervical carcinoma colonies. This encouraging result provides useful information for designing a much better anticancer compound using a plant-mediated synthesis of CuO NPs with minimal side effects.

Acknowledgments

This paper was supported by KU Research Professor Program, Konkuk University, Seoul, South Korea.
It was also partially supported by the Basic Science Research Program through the National Research Foundation of Korea (NRF) funded by the Ministry of Education (2015R1A2A2A01003741).

References

Abdel-Halim, E.S., El-Rafie, M.H., Al-Deyab, S.S., 2011. Polyacrylamide/guar gum graft copolymer for the preparation of silver nanoparticles. Carbohyd. Polym. 85, 692–697.

AshaRani, P.V., Low, K.M.G., Hande, M.P., Suresh, V., 2009. Cytotoxicity and genotoxicity of silver nanoparticles in human cells. ACS Nano 3, 279–290.

Awwad, A.M., Albiss, B.A., Salem, N.M., 2015. Antibacterial activity of synthesized copper oxide nanoparticles using *Malva sylvestris* leaf extract. SMU Med. J. 2, 91–100.

Bawadi, H.A., 2005. Inhibition of Caco-2 colon, MCF-7, and Hs578T breast, and DU 145 prostatic cancer cell proliferation by water-soluble black bean condensed tannins. Can. Lett. 218, 153–162.

Bhaumik, A., Shearin, A.M., Rishi, P., Kartik, G., 2014. Significant enhancement of optical absorption through nano-structuring of copper based oxide semiconductors: possible future materials for solar energy applications. Phys. Chem. Chem. Phys. 16, 11054–11066.

Bobe, G., Barret, K.G., Mentor-Marcel, R.A., Saffiotti, U., Young, M.R., Colburn, N.H., Albert, P.S., Bennink, M.R., Lanza, E., 2008. Dietary cooked navy beans and their fractions attenuate colon carcinogenesis in azoxymethane-induced Ob/Ob mice. Nutri. Cancer 60, 373–381.

Borgohain, J.B., Singh, M.V., Ramarao, T., Shripathi, S., Mahamuni, 2000. CuO: synthesis and characterization. Phys. Rev. 61, 11093–11096.

Brajesh, K., Smita, K.m., Luis, C., Alexis, D., Yolanda, A., 2015. Biofabrication of copper oxide nanoparticles using Andean blackberry (*Rubus glaucus* Benth.) fruit and leaf. Saudi Chem. Soc. http://dx.doi.org/10.1016/j.jscs.2015.01.009.

Cao, M., Wang, Y., Guo, C., Qi, Y., Hu, C., Wang, E., 2004. A simple route towards CuO nanowires and nanorods. J. Nanosci. Nanotechnol. 4, 824–828.

Chen, G., Zhou, H., Ma, W., Zhang, D., Qiu, G., Liu, X., 2011. Microwave-assisted synthesis and electrochemical properties of urchin-like CuO micro-crystals. Solid State Sci. 13, 2137–2141.

Cullity, B.D., 1978. Elements of X-ray Diffraction, second ed. Addison-Wesley, Massachusetts.

Dubey, S.P., Lahtinen, M., Sillanpa, M., 2010. Tansy fruit mediated greener synthesis of silver and gold nanoparticles. Process Biochem. 45, 1065–1071.

Dzomba, P., Togarepi, E., Mupa, 2013. Anthocyanin content and antioxidant activities of common bean species (*Phaseolus vulgaris* L.) grown in Mashonaland Central, Zimbabwe. Afr. J. Agri. Res. 8, 3330–3333.

Eliseev, A.A., Lukaskin, A.V., Vertegel, A.A., Heifets, L.I., Zhirov, A. I., Tretyakov, Y.D., 2010. Synthesis and characteristics of the copper nanoparticle. Mater. Res. Innov. 2000, 308–311.

Frankfurt, O.S., Krishan, A., 2003. Apoptosis-based drug screening and detection of selective toxicity to cancer cells. Antican. Drugs 14, 555–561.

Gao, D., Zhang, J., Zhu, J., Qi, J., Zhang, Z., Sui, W., Shi, H., Xue, D., 2010. Vacancy-mediated magnetism in pure copper oxide nanoparticles. Nanoscale Res. Lett. 5, 769–772.

Geil, P., Anderson, J., 1994. Nutrition and health implications of dry beans: a review. J. Am. Coll. Nutr. 13, 549–558.

GnanaDhas, G., Gurusamy, A., Chellapandian, K., 2012. Green synthesis of the silver nanoparticle using *Elettaria Cardamomom* and assessment of its antimicrobial activity. Int. J. Pharma Sci. Res. 3, 323–330.

Hajra, K.M., Liu, J.R., 2004. Apoptosome dysfunction in human cancer. Apoptosis 6, 691–704.

Hangen, L., Bennik, M.R., 2002. Consumption of black beans and navy beans (*Phaseolus vulgaris*) reduced azoxymethane-induced colon cancer in rats. Nutr. Cancer 44, 60–65.

Harland, B.F., Morris, E.R., 1995. Phytate: a good or a bad food component? Nutr. Res. 15, 733–754.

Huang, X., Wu, H., Pu, S., Zhang, W., Liao, X., Shi, B., 2011. One-step room-temperature synthesis of Au@Pd core–shell nanoparticles with the tunable structure using plant tannin as reductant and stabilizer. Green Chem. 13, 950–957.

Iovine, B., Oliviero, G., Garofalo, M., Orefice, M., Nocella, F., Borbone, N., Piccialli, V., Centore, R., Mazzone, M., Piccialli, G., Bevilacqua, M.A., 2014. The anti-proliferative effect of L-carnosine correlates with a decreased expression of hypoxia-inducible factor 1 alpha in human colon cancer cells. PLoS One 9, e96755.

Iravani, S., 2011. Green synthesis of metal nanoparticles using plants. Green Chem. 13, 2638–2650.

Irwin, J.C., Chrzanowski, J., Wei, T., 1990. Raman scattering from single crystals of cupric oxide. Physica C 166, 456–464.

Jayakumarai, G., Gokulpriya, C., Sudhapriya, R., Sharmila, G., Muthukumaran, C., 2015. Phytofabrication and characterization of monodisperse copper oxide nanoparticles using *Albizia lebbeck* leaf extract. Appl. Nanosci. 5, 1017–1021.

Sharma, Jitendra Kumar, Shaheer Akhtar, M., Ameen, S., Pratibha, S., Gurdip Singh, S., 2015. Green synthesis of CuO nanoparticles with leaf extract of *Calotropis gigantea* and its dye-sensitized solar cells applications. J. Alloys Comp. 632, 321–325.

Kumar, R., Dwivedi, P.D., Dhawan, A., Das, M., Ansari, M.K., 2011. Citrinin-generated reactive oxygen species cause cell cycle arrest leading to apoptosis via the intrinsic mitochondrial pathway in mouse skin. Toxicol. Sci. 2, 557–566.

Li, W., Bin, Z., Yong, Y.Z., XueJun, Z., QingDuan, W., LiXian, C., WenJun, Z., 2007. Syntheses of CuO nanostructures in ionic liquids. Sci. China Ser. B: Chem. 50, 63–69.

Lin, H.H., Wang, C.Y., Shih, H.C., Chen, J.M., Hsieh, C.T., 2004. Characterizing well-ordered CuO nanofibrils synthesized through gas-solid reactions. J. Appl. Phys. 95, 5889–5895.

Liu, Z., Kiessling, F., Gatjens, J., 2010. Advanced nanomaterials in multimodel imaging: design, functionalization, and biomedical applications. J. Nanomater. 2010, 894303.

Liu, P., Li, Z., Cai, W., Fang, M., Luo, X., 2011. Fabrication of cuprous oxide nanoparticles by laser ablation in PVP aqueous solution. RSC Adv. 1, 847–851.

Maestri, D.M., Nepote, V., Lamarque, A.L., Zygadlo, J.A., 2006. Natural products as antioxidants. Res. Signpost. 5, 105–135.

Mariappan, P., Krishnamoorthy, K., Kadarkaraithangam, J., Govindasamy, M., 2011. Selective toxicity of ZnO nanoparticles toward Gram-positive bacteria and cancer cells by apoptosis through lipid peroxidation. Nanomedicine 7, 184–192.

Mishra, S.B., Rao, C.V., Ojha, S.K., Vijayakumar, M., Verma, A., 2010. An analytical review of plants for anti diabetic activity with their phytoconstituent and mechanism of action: a review. Int. J. Pharmacol. Sci. Res. 1, 29–44.

Moktan, S., Raucher, D., 2012. Anticancer activity of proapoptotic peptides is highly improved by thermal targeting using elastin-like polypeptides. Int. J. Pept. Res. Ther. 18, 227–237.

Nasrollahzadeh, M., Sajadi, S. Mohammad, Rostami-Vartooni, A., Mehdi, K., 2015a. Green synthesis of Pd/Fe_3O_4 nanoparticles using *Euphorbia condylocarpa* M. bieb root extract and their catalytic applications magnetically recoverable and stable recyclable catalysts for the phosphine-free Sonogashira and Suzuki coupling reactions. J. Mol. Catal. A: Chem. 396, 31–39.

Nasrollahzadeh, M., Sajadi, S. Mohammad, Rostami-Vartooni, A., Mojtaba, B., 2015b. Green synthesis of Pd/CuO nanoparticles by *Theobroma cacao* L. seeds extract and their catalytic performance for the reduction of 4-nitrophenol and phosphine-free Heck coupling reaction under aerobic conditions. J. Coll. Int. Sci. 448, 106–113.

Nasrollahzadeh, M., Sajadi, S. Mohammad, Mehdi, M., 2015c. *Tamarix gallica* leaf extract mediated novel route for the green synthesis of CuO nanoparticles and their application for N-arylation of nitrogen-containing heterocycles under ligand-free conditions. RSC Adv. 5, 40628–40635.

Nasrollahzadeh, M., Mehdi, M., Sajadi, S. Mohammad, 2015d. Green synthesis of CuO nanoparticles by aqueous extract of Gundelia tournefortii and evaluation of their catalytic activity for the synthesis of N-monosubstituted ureas and reduction of 4-nitrophenol. J. Coll. Int. Sci. 455, 245–253.

Nasrollahzadeh, M., Maham., M., Rostami-Vartooni, A., Mojtaba, B., Sajadi, S. Mohammad, 2015e. Barberry fruit extract assisted *in situ* green synthesis of Cu nanoparticles supported on reduced graphene oxide–Fe_3O_4 nanocomposite as magnetically separable and reusable catalyst for the *O*-arylation of phenols with aryl halides under ligand-free conditions. RSC Adv. 5, 64769–64780.

Nasrollahzadeh, M., Sajadi, S. Mohammad, Honarmanda, E., Mehdi, M., 2015f. Preparation of palladium nanoparticles using *Euphorbia thymifolia* L. leaf extract and evaluation of catalytic activity in the ligand-free Stille and Hiyama cross-coupling reactions in water. New J. Chem. 39, 4745–4752.

Nasrollahzadeh, M., Sajadi, S. Mohammad, 2015. Preparation of Au nanoparticles by anthemis xylopoda flowers aqueous extract and their application for alkyne/aldehyde/amine A3-type coupling reactions. RSC Adv. 5, 46240–46246.

Nasrollahzadeh, M., Sajadi, S. Mohammad, Mehdi, M., 2015g. Green synthesis of palladium nanoparticles using Hippophae rhamnoides Linn leaf extract and their catalytic activity for the Suzuki-Miyaura coupling in water. J. Mol. Catal. A: Chem. 396, 297–303.

Nasrollahzadeh, M., 2014. Green synthesis and catalytic properties of palladium nanoparticles for the direct reductive amination of aldehydes and hydrogenation of unsaturated ketones. New J. Chem. 38, 5544–5555.

Pandurangan, M., Gansukh, E., Bhupendra, M., Murugesan, C., Rafi, N., Kim, D.H., 2015a. Investigation of the role of aspartame on apoptosis process in Hela cells. Saudi J. Biol. Sci. http://dx.doi.org/10.1016/j.sjbs.2015.06.01.

Pandurangan, M., Kim, D.H., Veerappan, M., Ravikumar, S., 2015b. Differential bio-potential of ZnS nanoparticles to normal mdck cells and cervical carcinoma Hela cells. J. Nanosci. Nanotechnol. 15, 1–8.

Rahnama, A., Gharagozlou, M., 2012. Preparation and properties of semiconductor CuO nanoparticles via a simple precipitation method at different reaction temperatures. Opt. Quant. Electron. 44, 313–322.

Rajgovind, Gaurav, S., Deepak, G., Nakuleshwar, D.J., Suresh, J., 2015. *Pterocarpus marsupium* derived phyto-synthesis of copper oxide nanoparticles and their antimicrobial activities. J. Microb. Biochem. Technol. 7, 140–144.

Rashad, M., Rüsing, M., Berth, G., Lischka, K., Pawlis, A., 2013. CuO and Co_3O_4 nanoparticles: synthesis, characterizations, and Raman spectroscopy. J. Nanomater., 6 Article ID 714853

Ren, G., Hu, D., Cheng, E.W., Vargas-Reus, M.A., Reip, P., Allaker, R.P., 2009. Characterization of copper oxide nano particles for antimicrobial applications. Int. J. Antimicrob. Agents 33, 587–590.

Saeed, J., Meissam, M., Ebrahim, R., 2014. Biological synthesis of zinc oxide and copper oxide nanoparticles. Int. Conf. Chem. Biomed. Environ. Eng. (ICCBEE'14) October 7–8, 2014 Antalya (Turkey).

Safarifard, V., Morsali, A., 2012. Sonochemical syntheses of a nano-sized copper (II) supramolecule as a precursor for the synthesis of copper (II) oxide nanoparticles. Ultrason. Sonochem. 19, 823–829.

Salah-Eddin, A.A., Nida, M.S., Ihab, H.G., Akl, M.A., 2015. Toxicity of nanoparticles against *Drosophila melanogaster* (Diptera: Drosophilidae). J. Nanomater., 9 Article ID 758132

Salavati, M., Davar, F., 2009. Synthesis of copper and copper (I) oxide nanoparticles by thermal decomposition of a new precursor. Mater. Lett. 63, 441–443.

Sangeetha, G., Sivaraj, R., Venckatesh, R., 2012. *Aloe barbadensis* Miller mediated green synthesis of mono-disperse copper oxide nanoparticles: optical properties. Spectrochim. Acta Part A: Mol. Biomol. Spectrosc. 97, 1140–1144.

Sankar Narayan, S., Dipak, P., Nilu, H., Dipta, S., Samir Kumar, P., 2015. Green synthesis of silver nanoparticles using fresh water green alga *Pithophora oedogonia* (Mont.) Wittrock and evaluation of their antibacterial activity. Appl. Nanosci. 5, 703–709.

Seigneuric, R., Markey, L., Nuyten, D.S.A., Dubernet, C., Evelo, C.T. A., Finot, E., Garrido, C., 2010. From nanotechnology to nanomedicine: applications to cancer research. Curr. Mol. Med. 10, 640–652.

Siddique, K., Karmakar, B., 2013. Study of structural and dielectric properties of copper oxide nanoparticles prepared by wet chemical precipitation method. Int. J. Nanosci. 12, 1350036–1350040.

Sivaraj, R., Pattanathu, K.S.M., Rahman, P., Rajiv, Abdul Salam, H., Venckatesh, R., 2014a. Biogenic copper oxide nanoparticles synthesis using *Tabernaemontana divaricate* leaf extract and its antibacterial activity against urinary tract pathogen. Spectrochim. Acta Part A: Mol. Biomol. Spectrosc. 133, 178–181.

Sivaraj, R., Pattanathu, K.S.M., Rahman, P., Rajiv, S., Narendhran, R., Venckatesh, 2014b. Biosynthesis and characterization of *Acalypha indica* mediated copper oxide nanoparticles and evaluation of its antimicrobial and anticancer activity. Spectrochim. Acta. Part A: Mol. Biomol. Spectrosc. 129, 255–258.

Shende, R., Subramanian, S., Hasan, S., Apperson, S., Thiruvengadathan, R., Gangopadhyay, K., Gangopadhyay, S., 2008. Nanoenergetic composites of CuO nanorods nanowires and Al-nanoparticles. Propell. Explos. Pyrot. 33, 122–130.

Sundaramurthy, N., Parthiban, C., 2015. Biosynthesis of copper oxide nanoparticles using *Pyrus pyrifolia* leaf extract and evolve the catalytic activity. Int. Res. J. Eng. Technol. 2, 332–337.

Swarnkar, R.K., Singh, S.C., Gopal, R., 2009. Synthesis of copper/copper–oxide nanoparticles optical and structural characterization. In: AIP Conference Proceedings (AIP Conf. Proc.). vol. 1147, pp. 205. http://dx.doi.org/10.1063/1.3183432.

Swarnkar, R.K., Singh, S.C., Gopal, R., 2011. Effect of aging on copper nanoparticles synthesized by pulsed laser ablation in water: structural and optical characterizations. Bull. Mater. Sci. 34, 1363–1369.

Tadjarodi, A., Roshani, R., 2014. A green synthesis of copper oxide nanoparticles by a mechanochemical method. Curr. Chem. Lett. 3, 215–220.

Tanaka, A., Onari, S., Arai, T., 1992. Raman scattering from CdSe microcrystals embedded in a germinate glass matrix. Phys. Rev. B 45, 6587–6592.

Tanaka, A., Onari, S., Arai, T., 1993. Low-frequency Raman scattering from CdS microcrystals embedded in a germanium dioxide glass matrix. Phys. Rev. B 47, 1237–1243.

Thompson, M.D., Mensack, M.M., Jiang, W., Zhu, Z., Lewis, M.R., McGinley, J.N., Brick, M.A., Thompson, H.J., et al, 2012. Cell signaling pathways associated with a reduction in mammary cancer burden by dietary common bean (*Phaseolus vulgaris* L.). Carcinogenesis 33, 226–232.

Umadevi, M., Christy, A.J., 2013. Synthesis, characterization and photocatalytic activity of CuO nanoflowers. Spectrochem. Acta A: Mol. Biomol. Spectrosc. 109, 133–137.

Vijay Kumar, P.P.N., Shameem, U., Pratap, K., Kalyani, R.L., Pammi, S.V.N., 2015. Green synthesis of copper oxide nanoparticles using *Aloe vera* leaf extract and its antibacterial activity against fish bacterial pathogens. BioNanoScience. http://dx.doi.org/10.1007/s12668-015-0171-z.

Wang, Z.Y., Chen, Z., 2000. Differentiation and apoptosis induction therapy in acute promyelocytic leukemia. Lancet Oncol. 1, 101–106.

Wang, H., Xu, J.Z., Zhu, J.J., Chen, H.Y., 2002. Preparation of CuO nanoparticles by microwave irradiation. J. Cryst. Growth 244, 88–94.

Wang, Z., Cheng, F., Megharaj, M., 2014. Characterization of iron–polyphenol nanoparticles synthesized by three plant extracts and their fenton oxidation of azo dye. ACS Sust. Chem. Eng. 2, 1022–1025.

Wu, Y.N., Chen, D.H., Shi, X.Y., et al, 2011. Cancer-cell-specific cytotoxicity of non-oxidized iron elements in iron core-gold shell NPs. Nanomedicine 7, 420–427.

Xu, J.F., Ji, W., Shen, Z.X., Tang, S.H., Ye, X.R., Jia, D.Z., Xin, X.Q., 2000. Preparation and characterization of CuO nanocrystals. J. Solid State Chem. 147, 516–519.

Xu, J.F., Ji, W., Shen, Z.X., Li, W.S., Tang, S.H., Ye, X.R., Jia, D.Z., Xin, X.Q., 1999. Raman spectra of CuO nanocrystals. J. Raman Spectrosc. 30, 413–415.

Yu, T., Cheong, F.C., Sow, C.H., 2004. The manipulation and assembly of CuO nanorods with line optical tweezers. Nanotechnology 15, 1732–1736.

Yu, Y., Zhang, J., 2009. Solution phase synthesis of rose like CuO. Mater. Lett 63, 1840–1843.

Zhan, G., Huang, J., Du, M., Abdul-Rauf, I., Ma, Y., Li, Q., 2011. Green synthesis of Au–Pd bimetallic nanoparticles: single-step bioreduction method with plant extract. Mater. Lett. 65, 2989–2991.

Zhu, J., Bi, H., Wang, Y., Wang, X., Yang, X., Lu, L., 2007. Synthesis of flower-like CuO nanostructures via a simple hydrolysis route. Mater. Lett. 61, 5236–5238.

Zhu, J., Chen, H., Liu, H., Yang, X., Lu, L., Wang, X., 2004. Mater. Sci. Eng. A 384, 172–176.